J. Fluid Mech. (2017), *vol.* 820, *pp.* 42–60. © Cambridge University Press 2017
doi:10.1017/jfm.2017.202

Slip-enhanced drop formation in a liquid falling down a vertical fibre

David Halpern[1] **and Hsien-Hung Wei**[2,†]

[1]Department of Mathematics, University of Alabama, Tuscaloosa AL 35487, USA

[2]Department of Chemical Engineering, National Cheng Kung University, Tainan 701, Taiwan

(Received 26 April 2016; revised 20 March 2017; accepted 27 March 2017;
first published online 2 May 2017)

For a liquid film falling down along a vertical fibre, classical theory (Kalliadasis & Chang *J. Fluid Mech.*, vol. 261, 1994, pp. 135–168; Yu & Hinch *J. Fluid Mech.*, vol. 737, 2013, pp. 232–248) showed that drop formation can occur due to capillary instability when the Bond number $G = \rho g a^3/\gamma h_0$ is below the critical value $G_c \approx 0.60$, where ρ is the fluid density, g is the gravitational acceleration, a is the fibre radius, γ is the surface tension and h_0 is the unperturbed film thickness. However, the experiment by Quéré (*Europhys. Lett.*, vol. 13 (8), 1990, pp. 721–726) found $G_c \approx 0.71$, which is slightly greater than the above theoretical value. Here we offer a plausible way to resolve this discrepancy by including additional wall slip whose amount can be measured by the slip parameter $\Lambda = 3\lambda/h_0$, where λ is the slip length. Using lubrication theory, we find that wall slip promotes capillary instability and, hence, enhances drop formation. In particular, when slip effects are strong ($\Lambda \gg 1$), the transition films and the drop height scale as $(c/\Lambda)^{-1/3}$ and $(c/\Lambda)^{2/3}$, respectively, distinct from those found by Yu & Hinch for the no-slip case where c is the travelling speed. In addition, for $\Lambda > 1$, G_c is found to increase with Λ according to $G_c \approx 0.7\Lambda^{1/3}$, offering a possible explanation why the G_c found by Quéré is slightly greater than that predicted by the no-slip model. Using the above expression, the estimated slip length in Quéré's experiment is found to be of the order of several micrometres, consistent with the typical slip length range 1–10 μm for polymeric liquids such as silicone oil used in his experiment. The existence of wall slip in Quéré's experiment is further supported by the observation that the film thinning kinetics exhibits the no-slip result $h \propto t^{-1/2}$ for early times and changes to the strong slip result $h \propto t^{-1}$, where h is the film thickness. We also show that when the film is ultrathin, although capillary instability can become further amplified by strong slip effects, the instability can be arrested by the equally intensified gravity draining in the weakly nonlinear regime whose dynamics is governed by the Kuramoto–Sivashinsky equation.

Key words: capillary flows, lubrication theory, thin films

† Email address for correspondence: hhwei@mail.ncku.edu.tw

1. Introduction

When a thin liquid film is coated on the surface of a fibre, it will undergo capillary instability (Bretherton 1961; Kalliadasis & Chang 1994; Kliakhandler, Davis & Bankoff 2001; Craster & Matar 2006; Ruyer-Quil *et al.* 2008; Kalliadasis *et al.* 2011). This instability is driven by surface tension and mainly arises from the circumferential curvature of the interface. Specifically, inevitable interfacial fluctuations will cause the circumferential Laplace pressures in the valleys to be higher than those in the troughs. As a result, the fluid in the valleys will be sucked toward the troughs, thereby amplifying the fluctuations and eventually making the film grow into large drops. If the fibre is placed in a vertical arrangement, capillary instability still persists. However, because of gravity, a drop gains (loses) an additional mass flow from the film behind (ahead of) the drop as it travels down the fibre (see figure 1). This continuous mass flow injection/ejection due to gravity will compete with the capillary flow due to surface tension, consequently affecting the resulting drop profile and travelling speed. This fibre coating problem has been studied both theoretically (Kalliadasis & Chang 1994; Yu & Hinch 2013) and experimentally (Quéré 1990), so the basic physics can be said to be well understood. However, there still exists a noticeable discrepancy between experiment and theory. This motivates us to revisit this problem to seek a plausible explanation to resolve this discrepancy. To see how the problem is motivated, we first look at experimental observations. Quéré (1990) conducted an experiment and found that such a flow can behave quite differently, depending on the film thickness. If the film is sufficiently thick, it will grow into bulges and turn into large drops. On the other hand, if the film thickness is below some critical value, bulges will be suppressed and maintain a steady shape. In other words, the film's growth can be inhibited by the saturation of the capillary instability. As the film thickness controls the relative importance between surface tension and gravitational forces, the Bond number characterizes the flow behaviour,

$$G = \frac{\rho g a^3}{\gamma h_0}, \tag{1.1}$$

where ρ is the fluid density, g is the gravitational acceleration, a is the fibre radius, γ is the surface tension and h_0 is the unperturbed film thickness. This dimensionless parameter can also be recognized as the velocity ratio of gravity-driven flow $\rho g h_0^2/\mu$ to capillary flow $(h_0/a)^3(\gamma/\mu)$, with μ being the fluid viscosity. As can be seen from (1.1), for given fluid and fibre radius, the unperturbed film thickness h_0 controls the magnitude of G critical to the dynamics of the film. For thick films such that G is small, surface tension dominates over gravity, thereby giving rise to drop formation due to capillary instability. On the other hand, if G is large when the film is sufficiently thin, the much stronger gravity force suppresses the capillary instability, thereby making the interface slightly undulated and advected with the falling flow. Hence, drop formation occurs if G is smaller than some critical value G_c. Quéré (1990) found $G_c \approx 0.71$. Similar drop formation and suppression can also occur to a pressure-driven core annular film flow where the behaviour of the interface is determined by the competition between surface tension and shear flow effects within the film (Kerchman 1995).

On the theoretical side, the common approach to modelling this fibre coating problem is by solving lubrication-type interfacial evolution equations. There are extensive studies along this line, showing that most features of this problem can be successfully captured by this method (Frenkel 1992; Kalliadasis & Chang 1994;

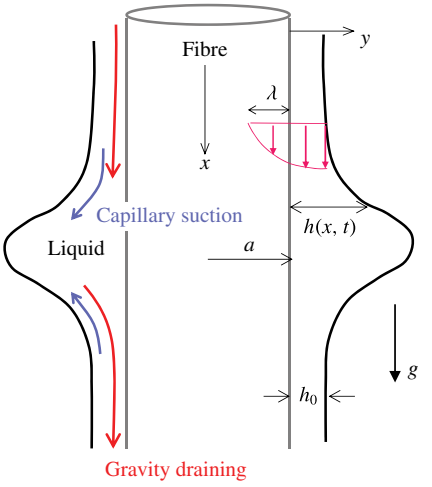

FIGURE 1. (Colour online) Sketch of a liquid film flowing down a slippery fibre of radius a and slip length λ. Owing to interplays between capillary suction and gravity draining, the film thickness $h(x, t)$ can vary with the axial position x and time t. Here h_0 is the unperturbed film thickness and g is the gravitational acceleration. In terms of dimensionless variables throughout this work, x and the transverse position y are scaled by a and h_0, respectively, and t is scaled by $3\mu a^4/\gamma h_0^3$.

Kerchman & Frenkel 1994; Kerchman 1995; Chang & Demekhin 1999; Kliakhandler *et al.* 2001; Duprat *et al.* 2007; Ruyer-Quil *et al.* 2008; Yu & Hinch 2013). Here we are more concerned with the critical Bond number G_c for an onset of drop formation. Kalliadasis & Chang (1994) first predicted $G_c \approx 0.60$ using a matched asymptotic theory. Yu & Hinch (2013) recently refined this result by including further corrections. In comparison, $G_c \approx 0.71$ found by Quéré (1990) is actually 18 % greater than the theoretical prediction $G_c \approx 0.60$. Although this discrepancy does not seem serious, it is nevertheless not unnoticeable. As the discrepancy here seems unlikely attributed to the lubrication model usually adopted, it could be that part of the inherent assumptions made in theory do not correspond to what happens in Quéré's experiment.

To see how the discrepancy arises, it is necessary to re-examine Quéré's experiment. He used silicone oil, a polymeric liquid that can exhibit considerable fluid slippage on a solid wall as it flows (de Gennes 1985; Brochard-Wyart *et al.* 1994). Together with the fact that the fibres here are made of nylon, which is hydrophobic, and could admit wall slip as well (due, for instance, to microbubbles trapped by surface microgrooves (Lauga, Brenner & Stone 2007)), it is likely that wall slip effects might no longer be negligible as usually considered. Previous studies showed that a variety of interfacial flows with wall slip could behave quite differently than those based on the no-slip boundary condition (Liao, Li & Wei 2013; Li *et al.* 2014; Liao *et al.* 2014; Halpern, Li & Wei 2015). In particular, in the related work by Liao *et al.* (2013), the authors found that a core annular film flow in a horizontal tube, even with a fractional amount of wall slip, can exhibit greater capillary instability than the usual no-slip case (Hammond 1983), especially when capillary draining proceeds to the stage where the film becomes thinner than the slip length. Recently, Haefner *et al.* (2015) experimentally examined the influence of slip on capillary instability of a thin liquid film on a horizontal fibre, showing that interfacial undulations with slip

do grow faster than those without slip. These studies imply that a thin, uniformly undulated film on a fibre would grow into bigger drops if wall slip is present. In other words, wall slip would facilitate drop formation by making drops start to appear at thinner films, which in turn makes the actual value of G_c greater than that without slip. This might explain why the experimental value $G_c \approx 0.71$ measured by Quéré (1990) is slightly greater than the theoretical value $G_c \approx 0.6$ predicted by the usual no-slip model (Kerchman & Frenkel 1994; Yu & Hinch 2013).

Motivated by the above, we examine in this paper how wall slip influences drop formation and interfacial dynamics for the fibre-coating problem. As will be shown shortly, wall slip not only enhances capillary instability resulting in bigger drops, but also leads G_c to increase with the amount of wall slip, making a falling liquid more susceptible to drop formation. We also find that even when slip effects are strong, it is still possible to prevent the film from growing to drops by saturating the capillary instability. In the following, we begin with the mathematical formation for this problem in § 2. In § 3, we derive new scalings for the strong slip situation in distinction to those for the no-slip case given by Yu & Hinch (2013). These strong slip scalings are also confirmed numerically. The general impact of wall slip on drop formation is presented in § 4. Connections to experiments will be made in § 5, showing that the discrepancy between experiment (Quéré 1990) and theory (Kerchman & Frenkel 1994; Yu & Hinch 2013) can be reasonably resolved by including additional slip effects.

2. Problem formulation

We follow the analysis of Yu & Hinch (2013) in deriving an evolution equation for the thickness of the liquid layer coating a vertical fibre of radius a. In order to apply the lubrication approximation, it is assumed that the film thickness is much smaller than the fibre radius, $h^* \ll a$, and that the change in thickness in the axial direction is also small, $|\partial h^*/\partial x^*| \ll 1$. The reduced momentum and continuity equations are

$$\mu u^*_{y^*y^*} = p^*_{x^*} - \rho g, \quad p^*_{y^*} = 0, \quad u^*_{x^*} + v^*_{y^*} = 0. \tag{2.1a–c}$$

Here (u^*, v^*) are the axial and transverse components of velocity, p^* is the pressure, and μ and ρ are the viscosity and density, respectively. Along the fibre, at $y^* = 0$, we apply the Navier slip and no-penetration conditions on the velocity field:

$$u^* = \lambda u^*_{y^*}, \quad v^* = 0, \tag{2.2a,b}$$

where λ is the slip length. At the free surface, $y^* = h^*(x^*, t^*)$, the balances of normal and tangential stresses are

$$p^* = \gamma \left(\frac{-h^*}{a} - h_{x^*x^*} \right) \tag{2.3}$$

and

$$\mu u^*_{y^*} = 0. \tag{2.4}$$

Note that just as in Yu & Hinch (2013), we have dropped the constant pressure term contribution that comes from the transverse component in curvature in (2.3) since it does not affect fluid motion, and we have applied the thin film approximation to the curvature of the surface. The kinematic boundary condition can be written as

$$h^*_{t^*} + Q^*_{x^*} = 0, \tag{2.5}$$

where $Q^* = \int_0^{h^*} u^* \, \mathrm{d}y^*$ is the axial flow rate. After integrating the momentum equation (2.1) and applying the boundary conditions (2.2) and (2.4), the following expression for the axial component of velocity is obtained:

$$u^* = \frac{1}{\mu}\left(p^*_{x*} - \rho g\right)\left[\frac{y^{*2}}{2} - h^* y^* - \lambda h^*\right]. \tag{2.6}$$

Thus,

$$Q^* = \frac{1}{3\mu}\left(\rho g - p^*_{x^*}\right)\left[h^{*3} + 3\lambda h^{*2}\right]. \tag{2.7}$$

As in Yu & Hinch (2013), we introduce the following dimensionless variables:

$$x = \frac{x^*}{a}, \quad h = \frac{h^*}{h_0}, \quad t = \frac{t^*}{\left(3\mu a^4/\gamma h_0^3\right)}, \quad p = \frac{p^*}{\gamma h_0/a^2}, \tag{2.8a–d}$$

where h_0 is the unperturbed film thickness. Thus, after substituting (2.3) and (2.7) in (2.5), and applying this non-dimensionalization, the kinematic boundary condition yields an evolution equation for the film thickness,

$$h_t + \left[\left(h^3 + \Lambda h^2\right)\left(G + h_x + h_{xxx}\right)\right]_x = 0, \tag{2.9}$$

where $\Lambda = 3\lambda/h_0$ is the slip parameter measuring the extent of wall slip relative to the unperturbed film thickness h_0. This equation has a travelling wave solution that can be determined by letting $x \to x - ct$ and $h(x, t) \to h(x - ct)$, where c is the propagating speed of the wave. Substituting the latter into (2.9) and integrating once with the uniform film condition $h \to 1$ as $x \to \pm\infty$, we obtain the following third-order equation for h:

$$-c\,(h-1) + \left(h^3 + \Lambda h^2\right)\left(G + h_x + h_{xxx}\right) = (1+\Lambda)\,G, \tag{2.10}$$

with

$$h \to 1 \quad \text{as} \quad x \to \pm\infty. \tag{2.11}$$

Equations (2.10) and (2.11) constitute an eigenvalue problem for $c(G, \Lambda)$, which is solved numerically using an iterative procedure similar to that in Yu & Hinch (2013). For completeness, some details of this method are provided in appendix A.

It is worth mentioning that as in Yu & Hinch (2013), the drop here is chosen to have a fixed length 2π (in the units of the fibre radius a), corresponding to the critical wavelength according to capillary instability (Hammond 1983). Perhaps it is more appropriate to choose the most unstable wavelength $2^{3/2}\pi$ to be the drop length (Kalliadasis & Chang 1994). Yu & Hinch (2013) found no differences between these two choices in terms of results. Also given that slip length does not change these two characteristic wavelengths for capillary instability (Liao *et al.* 2013), keeping the same drop length 2π should not change the features in the presence of wall slip.

3. Weak slip versus strong slip

Prior to presenting the overall influence of wall slip on the fibre-coating problem in § 4, it is instructive to gain some insights by inspecting scalings for both weak slip and strong slip limits. The weak slip ($\Lambda \ll 1$) limit recovers the no-slip results found previously (Yu & Hinch 2013). As will be shown below, how wall slip impacts drop formation is due to a length scale change of the short transition films that connect the uniform film to the main drop, as sketched in figure 2. This change will manifest most when slip effects are strong. Consequently, the scalings in the strong slip ($\Lambda \gg 1$) limit will be completely different from the no-slip ones, which will help explain the various features shown in § 4.

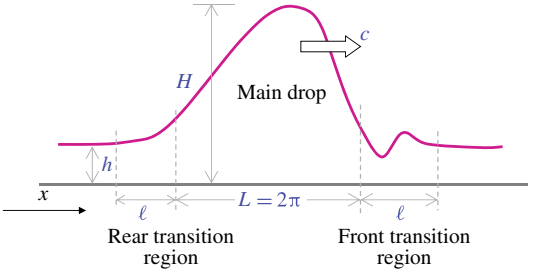

FIGURE 2. (Colour online) Sketch of main drop and two transition film regions.

3.1. *Weak slip limit*

In the weak slip ($\Lambda \ll 1$) limit, equation (2.10) reduces to the no-slip form (Yu & Hinch 2013):

$$-c\,(h-1)+G\left(h^3-1\right)+h^3\,(h_x+h_{xxx})=0. \tag{3.1}$$

Following the approach by Yu & Hinch (2013), we inspect the behaviour of the solutions in the transition film regions and the main drop region.

The length scale ℓ of the transition films is determined by balancing the travelling term ch to the axial interfacial curvature term $h^3h_{xxx}\sim h^4/\ell^3$. Because $h\sim O(1)$, this balance yields

$$\ell\sim c^{-1/3}. \tag{3.2}$$

This length scale is essentially obtained in a way similar to that in the classical Landau–Levich–Bretherton problem (Landau & Levich 1942; Bretherton 1961). Rescaling $z=c^{1/3}(x-x_0)$, equation (3.1) becomes

$$h_{zzz}=\frac{h-1}{h^3}-c^{-2/3}h_z+c^{-1}G\frac{1-h^3}{h^3}. \tag{3.3}$$

Hence, at leading order, equation (3.3) is simply governed by the Bretherton equation (Bretherton 1961).

When moving toward the main drop region, the axial interface curvature in the transition region $h_{xx}\sim\ell^{-2}$ has to match that of the main drop: $h_{max}/L^2\sim h_{max}$, giving

$$h_{max}\sim c^{2/3}(\gg 1). \tag{3.4}$$

So in the main drop region, rescaling the drop height $H=h/c^{2/3}$ with (3.4), equation (3.1) becomes

$$H_x+H_{xxx}=c^{-1}\left(H-c^{-2/3}\right)/H^3-c^{-2/3}G\left(1-c^{-2}/H^3\right). \tag{3.5}$$

As a result, the leading term is the curvature term on the left-hand side, meaning that at leading order the pressure in the main drop remains hydrostatic (Hammond 1983).

3.2. *Strong slip limit*

When wall slip is present and the slip length is large compared with the film thickness, we again use the balance $ch\sim\Lambda h^2h_{xxx}\sim\Lambda h^3/\ell^3$ to determine the length scale of the transition films as

$$\ell\sim\hat{c}^{-1/3}, \tag{3.6}$$

where $\hat{c} = c/\Lambda$. So the equation governing the transition films can be obtained by rescaling (2.10) with $\zeta = \hat{c}^{1/3}(x - x_0)$:

$$h_{\zeta\zeta\zeta} = \frac{h-1}{h^2\left(1+\Lambda^{-1}h\right)} - \hat{c}^{-2/3}h_\zeta + \hat{c}^{-1}G\left[\frac{1+\Lambda^{-1}}{h^2\left(1+\Lambda^{-1}h\right)} - 1\right]. \tag{3.7}$$

For large Λ, the leading order contribution in (3.7) is $h_{\zeta\zeta\zeta} = (h-1)/h^2$ (Liao *et al.* 2013; Li *et al.* 2014) provided that $\hat{c}$ is large. It follows that the main drop has a height of the order

$$h_{max} \sim \hat{c}^{2/3}. \tag{3.8}$$

Note that although $\Lambda \gg h$ in the transition films, the drop height h_{max} could still be much greater than the slip length, i.e. $\hat{c}^{2/3} \gg \Lambda$. In other words, unlike the situation in the films, in the main drop region the slip term $h^2\Lambda$ might not dominate over the h^3 term. Figure 3 shows that the calculated interface profile can be collapsed according to (3.6) and (3.8), confirming that both ℓ and h_{max} do change their scales when slip effects become strong.

Rescaling the drop height with $H = h/\hat{c}^{2/3}$ leads to the following equation for the main drop region:

$$H_x + H_{xxx} = \left(\frac{\Lambda}{\hat{c}}\right)\frac{H - \hat{c}^{-2/3} + \hat{c}^{-5/3}(1+\Lambda^{-1})G}{H^2\left(H + \dfrac{\Lambda}{\hat{c}^{2/3}}\right)} - \left(\frac{\Lambda}{\hat{c}}\right)^{2/3}\left(\frac{G}{\Lambda^{2/3}}\right). \tag{3.9}$$

Because $\Lambda \ll \hat{c}^{2/3}$ guarantees $\Lambda \ll \hat{c}$, the pressure in the drop is still hydrostatic at leading order, as it should be. If the first correction occurs at $O((\Lambda/\hat{c})^{2/3})$ due to gravity, G would have to be $O(\Lambda^{2/3})$ at most to establish a stable drop by balancing the drop weight to the capillary pressure difference between the top and bottom of the drop. Hence, for $\Lambda \gg 1$, how the critical Bond number G_c scales with Λ has to satisfy

$$G_c \sim \Lambda^n \quad \text{with } n \leqslant 2/3. \tag{3.10}$$

As will be shown later, we find $G_c \sim \Lambda^{1/3}$ (see (4.1)) which does satisfy the above criterion.

In appendix B, to see how wall slip impacts the fibre coating process in a more explicit manner, we have also looked at leading order effects in the transition films and analysed the modified Bretherton equation for arbitrary after rescaling the original equation (2.11) with the no-slip transition film length scale $c^{-1/3}$. As the equation is now only parameterized by Λ, its linearized solution exhibits a distinct asymptotic behaviour as the rescaled variable $z \to \pm\infty$. Having the asymptotic solution matched numerically with the main drop, we determine G_c and find that its value is virtually identical to that determined by the original equation (2.11). So this modified Bretherton equation suffices to capture the essence of this flow. More importantly, its asymptotic solution immediately reveals a factor of $\Lambda^{1/3}$ stretch for the transition films due to wall slip, which might explain $G_c \sim \Lambda^{1/3}$ found for the strong slip situation.

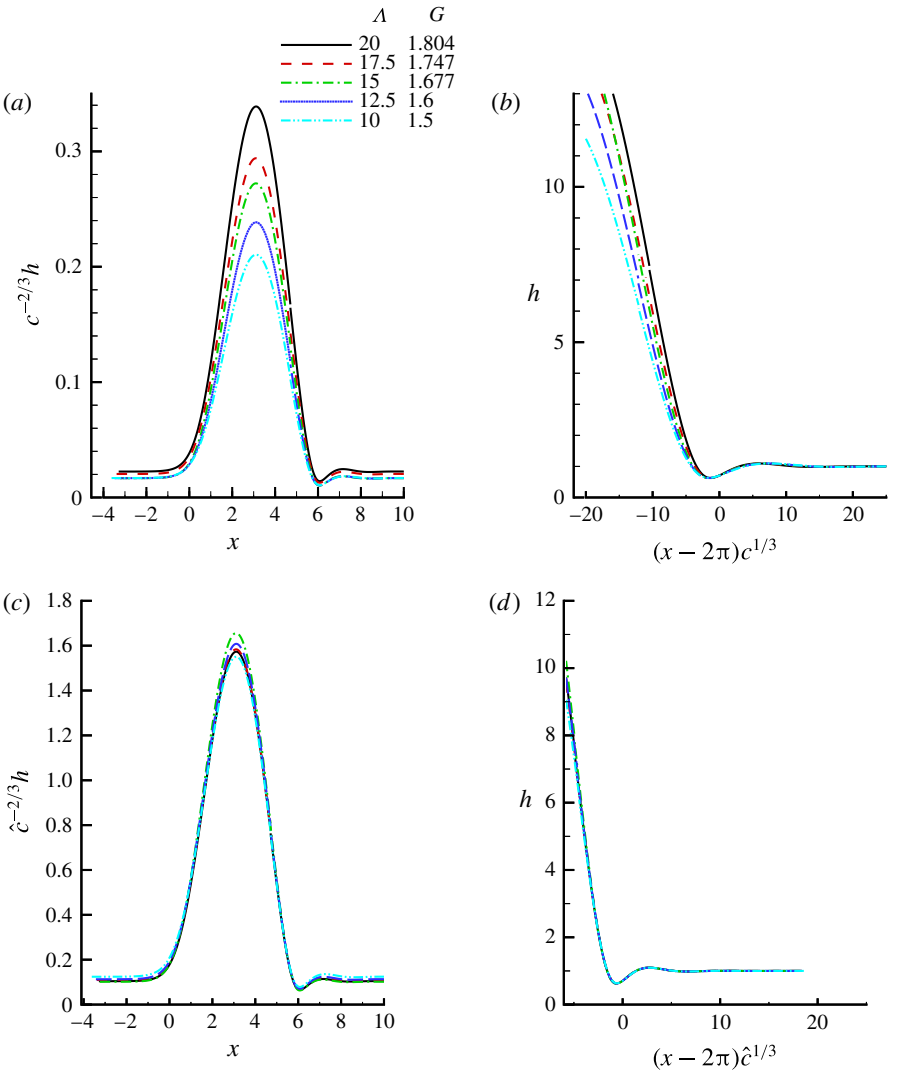

FIGURE 3. (Colour online) Numerical confirmations of strong slip scalings. (*a*) Plot of $hc^{-2/3}$ versus x and (*b*) plot of h versus $(x-2\pi)c^{1/3}$ (only for the front transition film region). Results are shown for various values of Λ and G along the decaying branch under the strong slip ($\Lambda \gg 1$) situation. Having h and x rescaled by the no-slip scalings (3.4) $h_{max} \sim c^{2/3}$ and (3.2) $\ell \sim c^{-1/3}$, respectively, we find that the curves do not collapse in any way, suggesting that h and x have to be rescaled differently. (*c*) Replot of (*a*) by plotting $h\hat{c}^{-2/3}$ versus x, where $\hat{c} = c/\Lambda$ is the rescaled wave speed. The result shows that all the curves in the main drop region collapse, confirming $h_{max} \sim \hat{c}^{2/3}$ according to (3.8). (*d*) Replot of (*b*) by plotting h versus $(x-2\pi)\hat{c}^{1/3}$. The result shows that all the curves in the transition film region collapse, confirming $\ell \sim \hat{c}^{-1/3}$ according to (3.6).

4. Impact of wall slip on drop formation

We first inspect how the interface shape changes with the amount of wall slip Λ. Figure 4 clearly reveals that for a given value of G, the drop height h_{max} significantly increases with Λ. In addition, the small 'dimple' ahead of the drop becomes deeper as

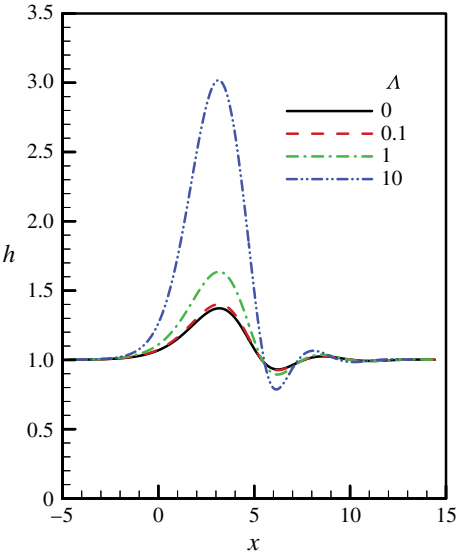

FIGURE 4. (Colour online) The interface profiles for various values of the slip parameter Λ. Here $G = 2$. The drop height increases as Λ increases.

Λ increases. These results can be explained by the much intensified capillary suction into the drop due to wall slip, in accordance with what was observed by Liao *et al.* (2013) for core annular film flow in a horizontal tube.

However, h_{max} is significantly suppressed by the gravitational effect since it decreases very rapidly as G is increased, as shown in figure 5. This is because for larger G the gravitational flow becomes stronger. Consequently, more fluid drains out of the drop, thus reducing the drop height. Note that an admissible travelling-wave solution that satisfies (2.10) with boundary condition (2.11) can only exist for G greater than the onset point for drop formation G_c. As also shown in figure 5, as Λ is increased, not only is h_{max} substantially amplified but also G_c is shifted to a larger value. The latter is because the thinner the film becomes, the more inclined it is to be influenced by wall slip, and hence more susceptible to drop formation.

The increase in the susceptibility to drop formation by wall slip becomes more evident by plotting the travelling-wave speed c against G. As shown in figure 6, the solution basically has two branches (Yu & Hinch 2013). One branch starts from G just above G_c, showing a rapid decay of c with G. This decaying branch continues to the point where c reaches a minimum c_{min} at some G. After that, the solution changes to the growing branch along which c increases with G. At $\Lambda = 0$, we get $G_c \approx 0.5960$ in agreement with Yu & Hinch (2013). Increasing Λ not only shifts G_c to a larger value, but also increases c considerably. So wall slip does not only promote drop formation, but also makes drops fall faster. Much faster falling drops can simply be explained by the significant increase in the drop weight due to the rise of h_{max} by wall slip (see figures 5 and 6).

How wall slip modifies the flow characteristics can be seen more clearly by plotting c_{min} against Λ in figure 7. At small Λ, weak slip merely makes c_{min} slightly greater than the no-slip case, and the increment here also slowly increases as Λ increases. So in the small Λ regime, we have $c_{min}(\Lambda \ll 1) \approx c_{min}(\Lambda = 0) + O(\Lambda)$. In the large Λ regime, however, increasing Λ makes c_{min} grow rather rapidly by following a linear

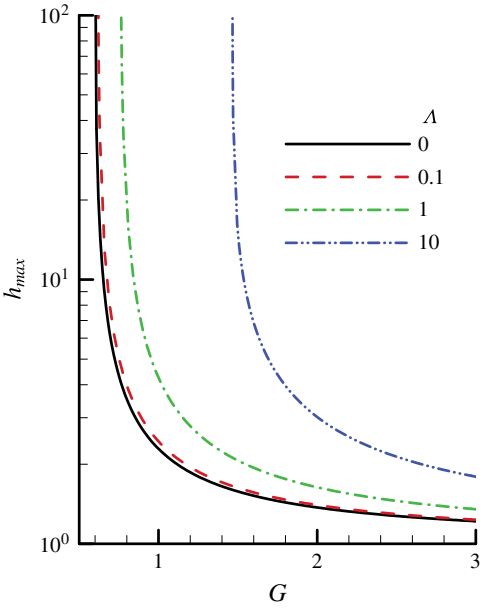

FIGURE 5. (Colour online) Plot of the drop height h_{max} versus G for various values of Λ shown in the figure. For a given value of Λ, h_{max} decreases rather rapidly as G is increased.

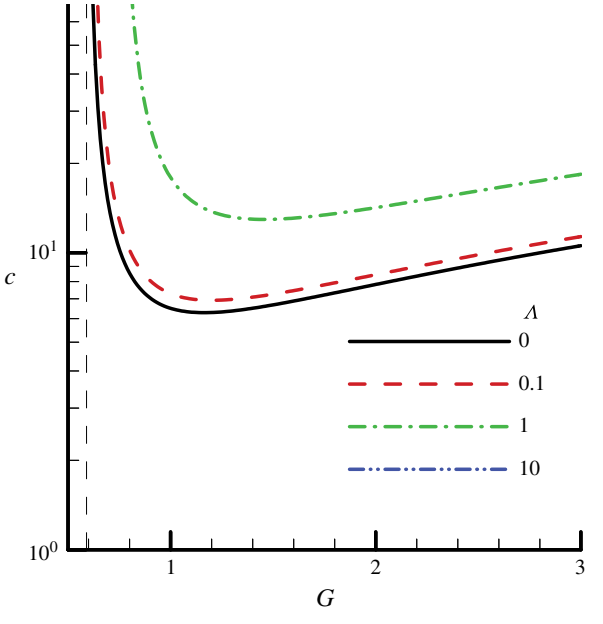

FIGURE 6. (Colour online) Plot of the wave speed c versus G for various values of Λ. For a given value of Λ, there are two solution branches: a decaying branch and a growing branch. These solutions exist for $G > G_c$. Increasing Λ makes G_c larger.

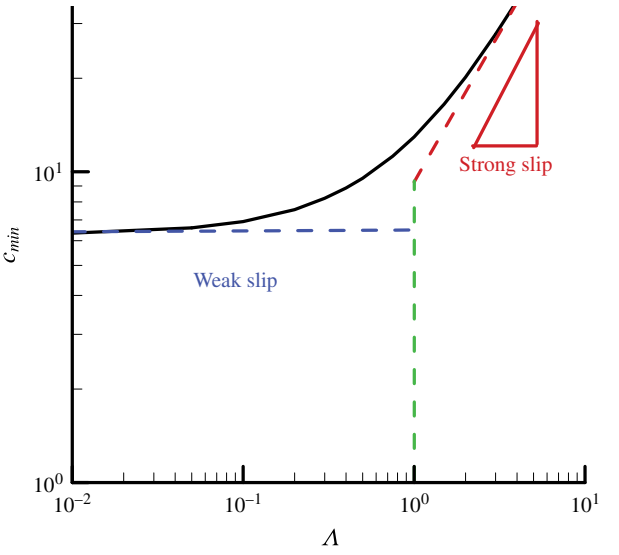

FIGURE 7. (Colour online) Plot of c_{min} versus Λ. In the weak slip ($\Lambda \ll 1$) limit, c_{min} is constant, while in the strong slip ($\Lambda \gg 1$) limit, c_{min} grows linearly with Λ. These two limits cross over at $\Lambda \sim 1$, the stick–slip transition point.

asymptote $c_{min}(\Lambda \gg 1) \approx k\Lambda$ with k being a numerical constant. This linear asymptote seems to be reminiscent of the result that c along the growing branch behaves as $c = (3 + 2\Lambda)G + 1.216(1 + \Lambda)$. The crossover between these two trends occurs at around $\Lambda \sim 1$, corresponding to the stick-to-slip transition point when the undisturbed film thickness h_0 turns from being thicker to being thinner than the slip length λ. This flow characteristic change due to wall slip is actually a generic feature for interfacial thin film flows when wall slip is present (Liao *et al.* 2013).

Figure 8 shows how G_c varies with Λ. Again, similar to how c_{min} varies with Λ in figure 7, G_c can vary with Λ in different ways when no slip changes to strong slip. For $\Lambda < 1$, G_c is roughly a constant, $G_c \approx 0.5960$, just like the no-slip result found by Yu & Hinch (2013). However, for $\Lambda > 1$, we find that G_c grows with Λ, which can be numerically fitted by

$$G_c \approx 0.7\Lambda^{1/3} \quad \text{for } \Lambda > 1, \tag{4.1}$$

and satisfies the criterion (3.10). The $\Lambda^{1/3}$ factor should be expected to come from the strong-slip transition film scale $O(\Lambda^{1/3}c^{-1/3})$ according to (3.6).

To sum up, wall slip causes: (i) the drop height h_{max} to become amplified; (ii) the drop falling speed c to be faster; and (iii) the onset point for drop formation G_c to be shifted to a larger value. Next, we look at the ultrathin film scenario to see how the strong tendency to drop formation due to wall slip is suppressed by gravity draining.

5. Ultrathin film scenario: suppression of capillary instability

When the film is thin, G is large. In this case, a much stronger gravity draining reduces the amplitude of the undulated interface, thereby preventing the film from growing into drops. In other words, large G tends to suppress capillary instability that causes drop formation. Specifically, because G does not affect the linear growth rate

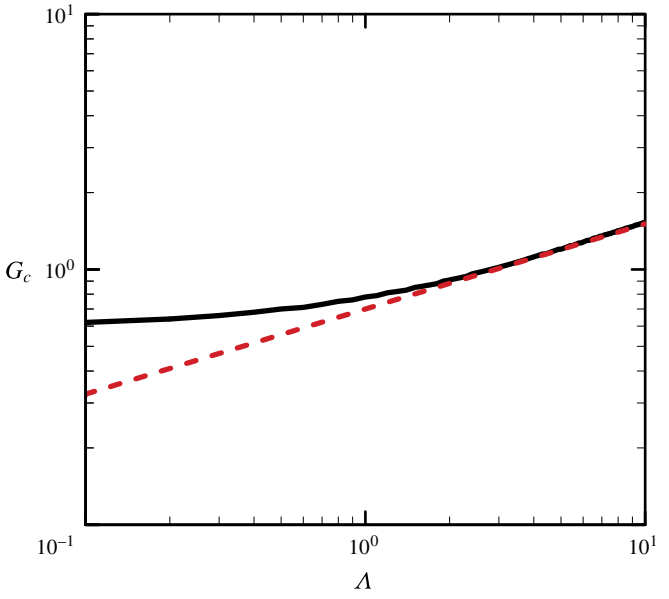

FIGURE 8. (Colour online) Plot of the critical Bond number G_c versus Λ in a log–log scale. The solid line is the calculated result. The dashed line is numerically fitted with $G_c = 0.7\Lambda^{1/3}$ for the data in the large Λ regime.

of the capillary instability, such suppression can only happen in the nonlinear regime in such a way that the nonlinear term in (5.2) (see below) steepens the waves to shortwaves, which, in turn, stabilize the capillary instability. This is the well-known Kuramoto–Sivashinsky (KS) mechanism that can saturate capillary instability in the weakly nonlinear regime, and hence prevent the film from growing into drops.

On the other hand, a very thin film also renders a large Λ, which promotes capillary instability by amplifying the interface's amplitude. Hence, there is a competition between slip-enhanced capillary instability and its nonlinear suppression by gravity draining. We therefore surmise that if G is sufficiently large, gravity draining might compensate the intensified capillary instability set up by wall slip, which might still prevent the film from growing to drops.

To test the above idea, instead of solving (2.10) to find a solitary wave solution, we solve the interfacial evolution equation (2.9) directly to see whether the slip-intensified capillary instability can be arrested for a very thin liquid film (i.e. large G). Figure 9 displays the calculated spatiotemporal interfacial evolution. It shows that even when a large Λ tends to promote capillary instability, a sufficiently large G (i.e. using a sufficiently large fibre) is able to substantially reduce the height of the liquid film and hence prevents it from developing into a drop.

To see how this interfacial suppression arises, we let $h = 1 + \eta$ with $|\eta| \ll 1$ to reduce (2.9) to the following weakly nonlinear equation:

$$\eta_t + (3 + 2\Lambda)\, G\eta_x + 2\,(3 + \Lambda)\, G\eta\eta_x + (1 + \Lambda)\,(\eta_{xx} + \eta_{xxxx}) = 0. \tag{5.1}$$

Here we neglect the non-linear correction $[\eta(\eta_x + \eta_{xxx})]_x$ to the capillary term, which will be justified *a posteriori*. Looking at the interface's dynamics in a moving

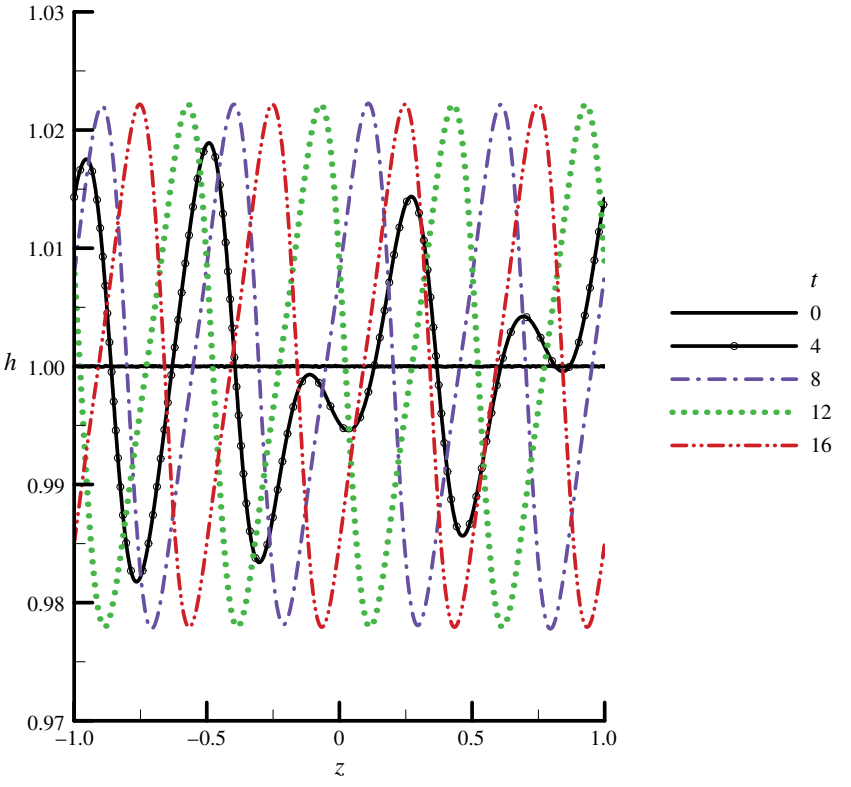

FIGURE 9. (Colour online) Calculated spatiotemporal interfacial evolutions of (2.9) with $\Lambda = 10$ and $G = 50$. While a large Λ tends to promote capillary instability, a sufficiently large G is able to substantially reduce the height of the liquid film and, hence, prevents it from developing into a drop. Here $z = 2x/L_1 - 1$ with $L_1 = 10\pi$.

frame of reference $\partial/\partial\tau = \partial/\partial t' + (3 + 2\Lambda)G\partial/\partial x$ with rescaled time $t' = t(1 + \Lambda)$, equation (5.1) can be re-written as

$$\eta_t + S\eta\eta_x + \eta_{xx} + \eta_{xxxx} = 0, \tag{5.2}$$

where $S = 2(3 + \Lambda)G/(1 + \Lambda)$. Equation (5.2) is the KS equation commonly seen in thin film flows (Frenkel 1992). It also indicates that wall-slip does not change the most unstable wavelength at all for capillary instability, just like the case with a stationary film (Liao *et al.* 2013). For large G, capillary instability can start to be saturated when η grows to the stage where the nonlinear wave steepening term $S\eta\eta_x$ becomes comparable to the circumferential curvature η_{xx} responsible for the instability. This leads the interface's amplitude to be bounded with a size $\eta \sim S^{-1}(\ll 1)$. The nonlinear correction to the capillary term is $O(S^{-2})$, and thus negligible. As a result, the strong slip case has $\eta(\Lambda \gg 1) \sim (2G)^{-1}$, three times larger than the no-slip case $\eta(\Lambda = 0) \sim (6G)^{-1}$. We solve (2.9) and compare the result with that of (5.1). Figure 10 shows excellent agreement between these two, confirming that while the interface can grow to a larger amplitude due to wall slip, the growth is still restrained by the KS mechanism described above.

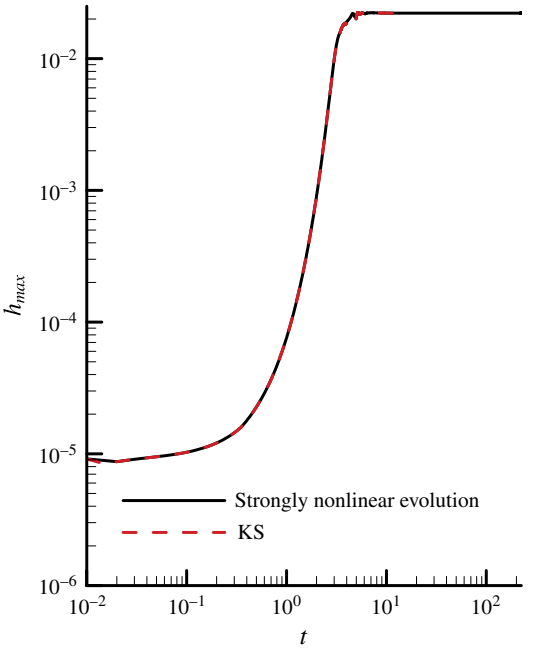

FIGURE 10. (Colour online) Comparison of simulation results between (2.9) and the weakly nonlinear equation (5.2), with $\Lambda = 10$, $G = 50$.

6. Connections to experiments

Quéré (1990) employed silicone oil in his fibre coating experiment and found $G_c = 0.71$. However, the no-slip theory predicts a slightly smaller value $G_c = 0.5960$ (Kalliadasis & Chang 1994; Yu & Hinch 2013). A plausible cause for this discrepancy might be attributed to the fact that silicone oil is a polymeric liquid capable of producing apparent wall slip. We have shown that G_c can be increased by wall slip according to (4.1). Using $G_c = 0.71$ and (4.1) to estimate the amount of wall slip in Quéré's experiment, we find $\Lambda \approx 1.043$. Taking $h_0 \approx 20$ μm seen in Quéré's experiment, the slip length $\lambda = \Lambda h_0/3$ is about 7.0 μm. This is within the typical slip length range of 1–10 μm for polymeric liquids (Brochard-Wyart *et al.* 1994).

It is worth mentioning that Chen (1988) used silicone oils to conduct a drop spreading experiment. He found that for the capillary number $Ca < 3 \times 10^{-5}$, the measured dynamic contact angle roughly scales as $\theta \sim Ca^{1/2}$, noticeably deviated from the no-slip result $\theta \sim Ca^{1/3}$ found for $Ca > 3 \times 10^{-5}$. Li *et al.* (2014) attributed this anomalous 1/2 power law to apparent wall slip caused by silicone oil. Based on the work by Brochard-Wyart *et al.* (1994), Li *et al.* (2014) estimated the slip length λ, and found that it can be as large as 10 μm. Because the viscosity (1960 mPa s) in Chen's experiment is comparable to that in Quéré's (500 mPa s), a similar amount of wall slip should exist in Quéré's experiment. Indeed, the estimated $\lambda \approx 7.0$ μm in the latter is close to $\lambda \approx 10$ μm in the former.

To test the $\Lambda^{1/3}$ factor in (4.1), slip effects can be made strong if a much thinner film is used. Since G_c increases with Λ according to (4.1), the fibre does not have to be thin for drop formation to be observed. Choosing $\Lambda \approx 30$ by taking $h_0 \approx 700$ nm, which is much thinner than $\lambda \approx 7$ μm, equation (4.1) gives $G_c \approx 2.17$. With the capillary length $\kappa^{-1} = (\gamma/\rho g)^{1/2} = 1.5$ mm used in Quéré's experiment, the above

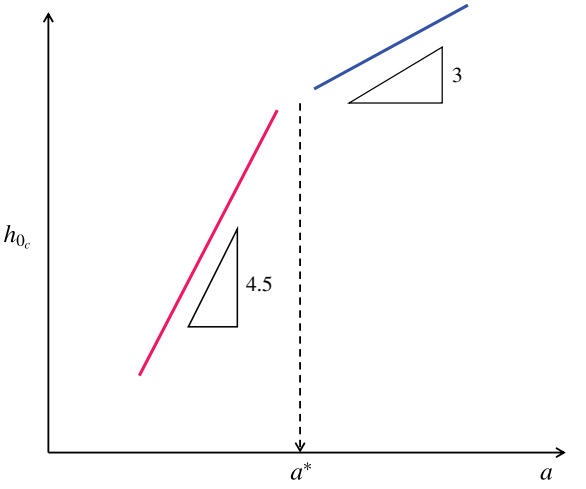

FIGURE 11. (Colour online) Sketch of how the critical film thickness h_{0c} varies with the fibre radius a (in log–log scale). For large fibres with $a > a^*$, the no-slip result $h_{0c} \propto a^3$ dominates (see (6.2)). However, if the fibre size is reduced to $a < a^*$, the strong-slip result $h_{0c} \propto a^{9/2}$ will dominate instead (see (6.1)), where $a^* = (\lambda\kappa^{-2})^{1/3}$ marks the critical fibre radius for the stick–slip transition with $\kappa^{-1} = (\gamma/\rho g)^{1/2}$ being the capillary length.

value of G_c yields a fibre of radius $a \approx 150$ μm. So one can vary both h_0 and a around the above values to see whether $h_{0c} \propto a^{9/2}$ according to $G_c \sim \Lambda^{1/3}$ in the strong slip regime. Moreover, to ensure $h_0 < \lambda$ in order to observe $h_{0c} \propto a^{9/2}$, the fibre radius needs to be chosen below 150 μm $\times$ $(7.0/0.7)^{1/9} \approx 194$ μm. Beyond this value, one will enter the no-slip regime. In other words, when varying a from small to large values, one might see that h_{0c} first exhibits the strong-slip result, $h_{0c} \propto a^{9/2}$ for small a, which then turns into the no-slip result $h_{0c} \propto a^3$ for large a. More precisely, when plotting h_{0c} against a as sketched in figure 11, one observes a transition from strong slip to no slip according to

$$\text{Strong slip: } h_{0c} \sim a^{9/2}/\left(\kappa^{-3}\lambda^{1/2}\right) \quad \text{for } a < a^*, \tag{6.1}$$

$$\text{No slip: } h_{0c} \sim a^3/\kappa^{-2} \quad \text{for } a > a^*, \tag{6.2}$$

where $a^* = (\lambda\kappa^{-2})^{1/3}$ marks the critical fibre radius for the slip-to-no-slip transition.

Another way to see how wall slip affects the coating is to look at the short-term film thinning kinetics. Neglecting the surface tension terms (i.e. omitting undulations of the interface), equation (2.9) is reduced to

$$h_t + \left(h^3 + \Lambda h^2\right)_x G = 0. \tag{6.3}$$

For small Λ, $h_t + G(h^3)_x = 0$ leads the film to thin according to $h \propto t^{-1/2}$, just like what Quéré observed. But when the film thins to the point where it becomes thinner than λ, the thinning kinetics is governed by $h_t + \Lambda G(h^2)_x = 0$. This accelerates the thinning to $h \propto t^{-1}$, which is close to the data trend for later times as seen in figure 12 reported by Quéré. Quéré attributed this thinning acceleration to axial grooves on the fibres. Alternatively, this acceleration can be interpreted by slip effects. The slip effects here could be caused by the hydrophobic fibres made by nylon, surface grooves, the silicone oil or their combination. Together with the fact that the measured $G_c = 0.71$ is slightly greater than $G_c = 0.5960$ for no-slip fibres, all these deviations found in Quéré's experiment can be well explained by wall slip effects.

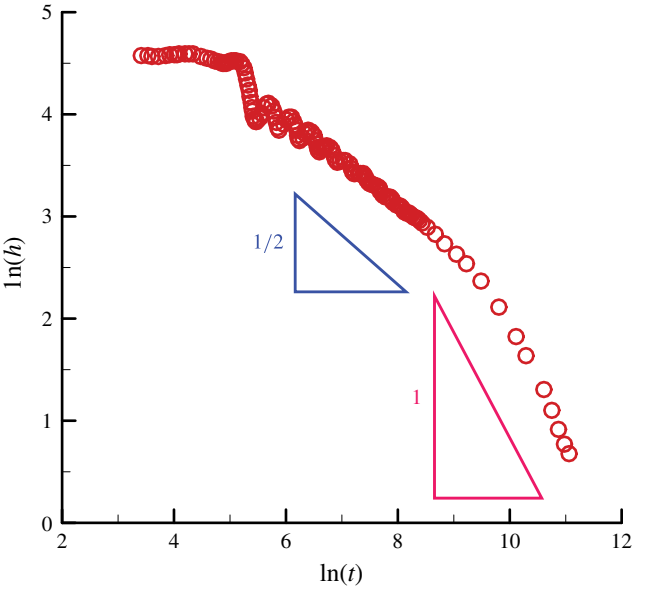

FIGURE 12. (Colour online) Temporal evolution of the film thickness measured by Quéré (1990), adapted from his figure 1. The film thinning kinetics can be accelerated from no-slip $h \propto t^{-1/2}$ to strong slip $h \propto t^{-1}$ at late times.

7. Concluding remarks

We have demonstrated that wall slip can promote drop formation along a vertical fibre. Both the drop height and falling speed can be significantly increased with the amount of wall slip. In particular, when slip effects become strong, the critical Bond number G_c for drop formation is found to increase with Λ as $G_c \approx 0.7\Lambda^{1/3}$. The $\Lambda^{1/3}$ factor then leads the critical film thickness to vary with the fibre radius as $h_{0c} \propto a^{9/2}$, more sensitive than the no-slip result $h_{0c} \propto a^3$. Such a sensitivity to the fibre radius due to wall slip explains why G_c found by Quéré (1990) is slightly greater than that predicted by the no-slip model. The $\Lambda^{1/3}$ factor might come from changes of two length scales when wall slip effects become strong: (i) $O(\Lambda^{1/3}c^{-1/3})$ for the transition film regions ahead and behind the main drop; and (ii) $O(\Lambda^{-2/3}c^{2/3})$ for the drop height. These are very distinct from those for the no-slip case in which the transition film regions are $O(c^{-1/3})$ and the drop height is $O(c^{2/3})$ (Yu & Hinch 2013). We also find that the film thinning kinetics can be accelerated from no-slip $h \propto t^{-1/2}$ to strong slip $h \propto t^{-1}$ at late times, in accordance with Quéré's experiment. When the film is ultrathin, although strong slip effects can amplify capillary instability to make the film more susceptible to drop formation, this effect can be inhibited by equally intensified gravity draining through the KS mechanism.

It is worth remarking that the present analysis is more suitable for the situation where apparent slip is generated by a polymeric liquid as in Quéré's experiment. For a flow over a rough or textured surface, however, the effective slip length can only be defined when the film is much thicker than the size of the roughness. Hence, if the film is much thinner than the size of roughness, our analysis will no longer be applicable.

Acknowledgement

This work was supported by the Ministry of Science and Technology of Taiwan under grant no. 105-2221-E-006-227-MY3 of H.-H.W.

Appendix A

The numerical method used to solve (2.10) is similar to that described in Yu & Hinch (2013). As the uniform film regions are approached, asymptotic solutions can be obtained by linearizing (2.10) about $h = 1$. Letting $h = 1 + \delta\eta$ where $\delta \ll 1$, to leading order η satisfies

$$\eta_{xxx} + \eta_x + \frac{1}{1+\Lambda}\left((3+2\Lambda)G - c\right)\eta = 0. \tag{A 1}$$

This equation has solutions of the form e^{mx} where m satisfies the cubic equation

$$m^3 + m + \frac{1}{1+\Lambda}\left((3+2\Lambda)G - c\right) = 0. \tag{A 2}$$

If the constant term of the cubic is positive, that is when $c < (3+2\Lambda G)$, this equation has one positive real root, m_+, which yields an exponentially decaying solution as $x \to -\infty$ of the form $A\mathrm{e}^{m_+ x}$, and two complex conjugate roots with negative real parts, $\alpha \pm \mathrm{i}\beta$, that give rise to two oscillatory solutions that decay as $x \to \infty$ of the form $B\mathrm{e}^{\alpha x}\cos(\beta x + k)$ where A, B and k are constants.

Equation (2.10) is rewritten as a system of three first-order differential equations, and solved as an initial value problem using a Runge–Kutta method (ODE45 from MATLAB). Let h_1 be the solution of (2.10) with the initial condition specified at $x = -d_1$ coming from the monotonically decaying solution as $x \to -\infty$, and let h_2 be the solution of (2.10) with the initial condition specified at $x = d_2$ coming from the oscillatory decaying solution as $x \to \infty$. We stop computing h_1 and h_2 at $x = d$, a point in the middle of the drop where h is not too close to 1, and require h and h_x to be continuous and $h_{xx} = 0$ there, i.e. $h_1(d) = h_2(d)$, $h_{1x}(d) = h_{2x}(d)$, $h_{1xx}(d) = 0$ and $h_{2xx}(d) = 0$. An iterative scheme based on a Newton's method is applied that adjusts the speed c and the amplitude of the oscillatory decaying solution until the matching conditions are satisfied.

Appendix B

Let $x = x_0 + c^{-1/3}\xi$. Then (2.10) becomes

$$h_{\xi\xi\xi} = \frac{h-1}{h^3 + \Lambda h^2} - c^{-2/3}h_\xi + c^{-1}G\frac{1 - h^3 + \Lambda(1-h^2)}{h^3 + \Lambda h^2}. \tag{B 1}$$

For $c \gg 1$, the leading order problem is

$$h_{\xi\xi\xi} = \frac{h-1}{h^3 + \Lambda h^2}. \tag{B 2}$$

The above equation is solved subject to matching conditions with the uniform film regions, where $h \to 1$. Letting $h = 1 + \delta\eta$ where $\delta \ll 1$, $\eta_{\xi\xi\xi} = \eta/(1+\Lambda)$, whose solutions are

$$\mathrm{e}^{\xi/(1+\Lambda)^{1/3}}, \quad \mathrm{e}^{-\xi/2(1+\Lambda)^{1/3}}\cos\left(\frac{\sqrt{3}}{2}\frac{\xi}{(1+\Lambda)^{1/3}}\right), \quad \mathrm{e}^{-\xi/2(1+\Lambda)^{1/3}}\sin\left(\frac{\sqrt{3}}{2}\frac{\xi}{(1+\Lambda)^{1/3}}\right). \tag{B 3a–c}$$

The appropriate asymptotic solution to match with the rear uniform film is the first one given in (B 3), which is a purely decaying mode there, while in the front uniform film, we retain the other two solutions since they decay as $\xi \to \infty$. From (B 2), in the large drop region, where $h \gg 1$, the curvature is constant to leading order. Also, the profiles approaching the large drop from either the front or rear transition regions can be described by parabolas of the form

$$h \sim \tfrac{1}{2}P_{\pm}\xi^2 + R_{\pm} = \tfrac{1}{2}c^{2/3}P_{\pm}(x - x_0)^2 + R_{\pm}, \tag{B 4}$$

where, by a suitable choice of the origin, equation (B 4) has no linear term in ξ. For a given Λ, equation (B 2) is solved numerically using the purely decaying mode given in (B 3) as an initial condition for the left transition region. This numerical solution is matched with the large constant curvature drop as $\xi \to \infty$, yielding values for P_+ and R_+. In the front (or right) transition region, the initial condition for h is expressed as a combination of the two oscillatory solutions in (B 3),

$$h \approx 1 + A_f \mathrm{e}^{-\xi/2(1+\Lambda)^{1/3}} \cos\left(\frac{\sqrt{3}}{2}\frac{\xi}{(1+\Lambda)^{1/3}} + \phi\right), \tag{B 5}$$

where A_f and ϕ are the amplitude (chosen to be small) and a phase difference. The latter provides an extra degree of freedom in comparison with the rear transition region. Numerically, it is adjusted using a Newton's method until $P_- = P_+$, so that the pressure is continuous.

As explained by Yu & Hinch (2013), from the perspective of the large drop, the constant terms in (B 4) denote the thicknesses of the uniform films. The critical G can be obtained from the following relationship

$$G = \frac{R_+ - R_-}{2\pi}. \tag{B 6}$$

REFERENCES

Bretherton, F. P. 1961 The motion of long bubbles in tubes. *J. Fluid Mech.* **10** (2), 166–188.

Brochard-Wyart, F., de Gennes, P.-G., Hervert, H. & Redon, C. 1994 Wetting and slippage of polymer melts on semi-ideal surfaces. *Langmuir* **10** (5), 1566–1572.

Chang, H. C. & Demekhin, E. A. 1999 Mechanism for drop formation on a coated vertical fibre. *J. Fluid Mech.* **380**, 233–255.

Chen, J.-D. 1988 Experiments on a spreading drop and its contact angle on a solid. *J. Colloid Interface Sci.* **122** (1), 60–72.

Craster, R. V. & Matar, O. K. 2006 On viscous beads flowing down a vertical fibre. *J. Fluid Mech.* **553**, 85–105.

Duprat, C., Ruyer-Quil, C., Kalliadasis, S. & Giorgiutti-Dauphine, F. 2007 Absolute and convective instabilities of a viscous film flowing down a vertical fibre. *Phys. Rev. Lett.* **98** (24), 244502.

Frenkel, A. L. 1992 Nonlinear theory of strongly undulating thin films flowing down vertical cylinders. *Europhys. Lett.* **18** (7), 583–588.

de Gennes, P.-G. 1985 Wetting: statics and dynamics. *Rev. Mod. Phys.* **57** (3), 827–863.

Haefner, S., Benzaquen, M., Baumchen, O., Salez, T., Peters, R., McGraw, J. D., Jacobs, K., Raphael, E. & Dalnoki-Veress, K. 2015 Influence of slip on the Plateau–Rayleigh instability on a fibre. *Nat. Commun.* **6**, 7409.

HALPERN, D., LI, Y.-C. & WEI, H.-H. 2015 Slip-induced suppression of Marangoni film thickening in surfactant-retarded Landau–Levich–Bretherton flows. *J. Fluid Mech.* **781**, 578–594.

HAMMOND, P. S. 1983 Nonlinear adjustment of a thin annular film of viscous fluid surrounding a thread of another within a circular pipe. *J. Fluid Mech.* **137**, 363–384.

KALLIADASIS, S. & CHANG, H.-C. 1994 Drop formation during coating of vertical fibres. *J. Fluid Mech.* **261**, 135–168.

KALLIADASIS, S., RUYER-QUIL, C., SCHEID, B. & VELARDE, M. G. 2011 *Falling Liquid Films,* vol. 176. Springer Science & Business Media.

KERCHMAN, V. 1995 Strongly nonlinear interfacial dynamics in core-annular flows. *J. Fluid Mech.* **290**, 131–166.

KERCHMAN, V. I. & FRENKEL, A. L. 1994 Interactions of coherent structures in a film flow – simulations of a highly nonlinear evolution equation. *Theor. Comput. Fluid Dyn.* **6** (4), 235–254.

KLIAKHANDLER, I. L., DAVIS, S. H. & BANKOFF, S. G. 2001 Viscous beads on vertical fibre. *J. Fluid Mech.* **429**, 381–390.

LANDAU, L. D. & LEVICH, V. G. 1942 Dragging of a liquid by a moving plate. *Acta Physicochim. USSR* **17**, 42–54.

LAUGA, E., BRENNER, M. P. & STONE, H. A. 2007 *Microfluidics: The No-Slip Boundary Condition*, pp. 1219–1240. Springer.

LI, Y. C., LIAO, Y. C., WEN, T. C. & WEI, H.-H. 2014 Breakdown of the Bretherton law due to wall slippage. *J. Fluid Mech.* **741**, 200–227.

LIAO, Y. C., LI, Y. C., CHANG, Y. C., HUANG, C. Y. & WEI, H.-H. 2014 Speeding up thermocapillary migration of a confined bubble by wall slip. *J. Fluid Mech.* **746**, 31–52.

LIAO, Y. C., LI, Y. C. & WEI, H.-H. 2013 Drastic changes in interfacial hydrodynamics due to wall slippage: slip-intensified film thinning, drop spreading, and capillary instability. *Phys. Rev. Lett.* **111** (13), 136001.

QUÉRÉ, D. 1990 Thin-films flowing on vertical fibres. *Europhys. Lett.* **13** (8), 721–726.

RUYER-QUIL, C., TREVELEYAN, P., GIORGIUTTI-DAUPHINÉ, F., DUPRAT, C. & KALLIADASIS, S. 2008 Modelling film flows down a fibre. *J. Fluid Mech.* **603**, 431–462.

YU, L. Y. & HINCH, J. 2013 The velocity of 'large' viscous drops falling on a coated vertical fibre. *J. Fluid Mech.* **737**, 232–248.